Properties and Sulfide Stress Cracking Resistance of Coarse-Grained Heat-Affected Zones in V-Microalloyed X60 Steel Pipe

The effect of weld cooling rates and postweld heat treatment on microhardness, microstructure, tensile properties, and sulfide stress cracking resistance was studied

BY J. E. RAMIREZ, S. MISHAEL, AND R. SHOCKLEY

ABSTRACT. Evaluation of heat-affected zone (HAZ) properties after postweld heat treatment (PWHT) is important not only for selection of suitable chemical composition of microalloyed steel pipes, but also for development of welding procedures, including PWHT, for sour service. In this study, coarse-grained heat-affected zones (CGHAZ) were induced in V-microalloyed X60 steel pipe specimens using a Gleeble weld thermal simulation. Cooling rates from 5 to 80°C/s were used to represent a broad range of welding conditions. The CGHAZ specimens were subjected to PWHT at temperatures from 635 to 670°C (1175 to 1238°F) for 3 to 15 hours. Microhardness and microstructure of the CGHAZ were evaluated in the simulated "as-welded" and PWHT condition as functions of weld cooling rate and PWHT schedule. The tensile properties and sulfide stress cracking resistance (SSC) of CGHAZ with selected hardness level were determined as well. The maximum hardness of the CGHAZ increases from 233 to 392 HV-10, and its microstructure changes from ferrite with aligned second phases to martensite by increasing the cooling rate from 5 to 80°C/s.

None of the PWHT schedules used in this study induced hardening of the CGHAZ of the microalloyed steel. However, the rate of softening may have been retarded because of VC secondary hardening. For a holding time between 3 and 15 hours, the softening effect induced by the PWHT can be described by the Larson-Miller tempering parameter. The apparent activation energy for tempering in the different softening regimes observed during PWHT was determined. The behavior of the CGHAZ during tensile testing depends on the degree of overmatching between the CGHAZ and the base material. Coarse-grained heat-affected zones with a maximum hardness of 264 HV did not crack during exposure to sour testing according to procedure specified in standard NACE TM0177 (Method A).

J. E. RAMIREZ is with Edison Welding Institute. S. MISHAEL and R. SHOCKLEY are with ChevronTexaco Energy Technology Company.

Introduction

During welding, the HAZ of base metals is subjected to thermal cycles, which produces a change in both its microstructure and mechanical properties. In addition to chemical composition, rate of cooling through the temperature range within which transformation of austenite occurs to martensite, bainite, ferrite plus pearlite, or mixtures of these microstructural constituents, has a marked influence on the hardness achieved for a particular composition. The cooling time $\Delta t_{8\text{-}5}$ through the range 800° to 500°C, as descriptive of a given weld, has been widely adopted in the welding community as an important index. The temperature of 800°C, in most steels, approximately represents the A_3 transformation temperature and the γ/α transformation takes place through the 800° to 500°C temperature range.

For single-pass welds in C-Mn and low-carbon microalloyed steels, four microstructural regions can be distinguished in the HAZ as indicated in Fig. 1. The microstructure in each region of the HAZ is related to the temperature cycle experienced during welding. The four general regions and their corresponding temperature ranges are as follows:

- Coarse-grained HAZ (CGHAZ) – 1100°C to melting point
- Fine-grained HAZ (FGHAZ) — Ac_3–1100°C
- Intercritical HAZ (ICHAZ) — Ac_1–Ac_3
- Subcritical HAZ (SC-HAZ) — Below Ac_1

In multipass welds in C-Mn steels, each of the HAZ regions can experience multiple temperature excursions that can further alter the microstructure in the HAZ. For convenience, these regions can be categorized into six basic types as compared to four in single-pass welding. The two extra basic regions are as follows: intercritically reheated CGHAZ (IC-CGHAZ) and subcritically reheated CGHAZ (SC-CGHAZ). The mechanical properties vary across the different subzones. Among the HAZ subzones, the CGHAZ, which experiences the most severe thermal cycle, usually possesses the maximum hardness. As such, this region is usually given the most attention regarding alloy design and welding procedure, including PWHT.

Postweld heat treatment is commonly applied to welded steel construction for three main reasons. First, it may be deemed necessary to improve the mechanical properties, in particular the toughness, across the welds (Ref. 1). Second, heat treatment is applied to reduce the high level of residual stresses that are induced along and across weldments (Ref. 1, 2). Third, PWHT is used to decrease the hardness across the weldment to avoid the risk to stress corrosion cracking (SCC) (Ref. 1), for example, hardness level below 22 HRC in sour service. According to the provisions established in the NACE material recommendations for sour service (MR0175) (Ref. 3), a maximum hardness of 22 HRC (248 HVN) is recommended to avoid the risk to sulfide stress cracking.

The changes in strength, hardness, and toughness during PWHT are the net re-

KEYWORDS

Heat-Affected Zone (HAZ)
Postweld Heat Treatment (PWHT)
Coarse-Grained Heat-Affected Zones (CGHAZ)
Sulfide Stress Cracking Resistance (SSC)
V-Microalloyed X60 Steel Pipe
Larson-Miller Tempering Parameter

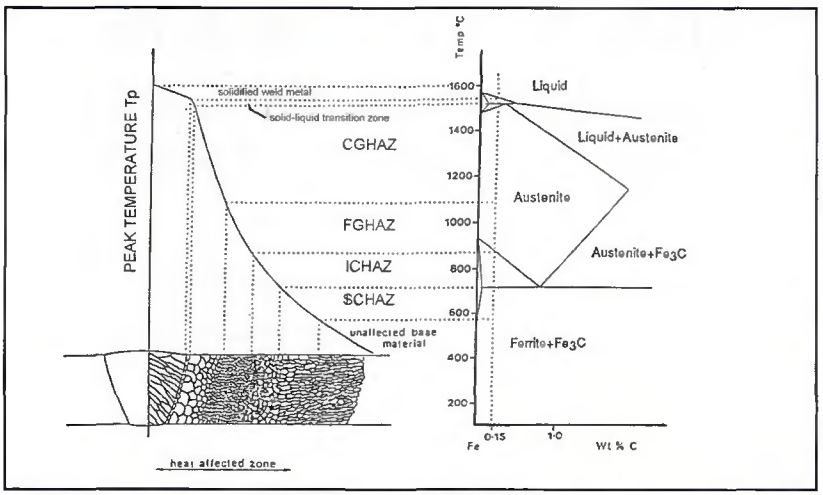

Fig. 1 — A schematic illustration of the various single-pass HAZ regions with reference to the iron-carbon equilibrium diagram. (An Fe-0.15 wt-% carbon steel is shown.)

Table 1 — Chemical Composition, Weight Percent, of the V-Microalloyed Seamless X60 Steel Pipe

Element	C	Si	Mn	P	S	Al	Cu	Cr
%	0.13	0.24	1.31	0.009	0.004	0.038	0.09	0.13
Element	Ni	Mo	V	Ti	Nb	N	B	Ca
%	0.1	0.2	0.052	0.002	0.001	0.011	0.0001	0.0004

Ceq: 0.44
V + Ti + Nb: 0.055

Table 2 — PWHT Schedules Imposed on the CGHAZ Specimens

PWHT	Specimens	Nominal Description	Actual PWHT
1	12, 16, 20, 24	635°C for 15 h	636.4 ± 4.3°C for 15.27 h
2	13, 17, 21, 25	635°C for 12 h	634 ± 3.3°C for 12.03 h
3	14, 18, 22, 26	635°C for 6 h	634.8 ± 2.5°C for 6.06 h
4	15, 19, 23, 27	635°C for 3 h	636.3 ± 4.2°C for 3.16 h
5	28, 38, 48, 58	650°C for 15 h	652 ± 1.9°C for 15.25 h
6	29, 39, 49, 59	650°C for 12 h	651.1 ± 2.8°C for 12.1 h
7	30, 40, 50, 60	650°C for 6 h	653.7 ± 2.2°C for 6.14 h
8	31, 41, 51, 61	650°C for 3 h	652.2 ± 2.8°C for 3.14 h
9	33, 42, 52, 62	670°C for 15 h	673.7 ± 4.4°C for 15.25 h
10	34, 43, 53, 63	670°C for 12 h	675 ± 4.5°C for 12.14 h
11	35, 44, 54, 64	670°C for 6 h	672.6 ± 1.7°C for 6.14 h
12[a]	36, 45, 55, 65	670°C for 3 h	680 ± 5°C for 3.26 h
13[a]	32, 47, 57, 67	670°C for 3 h	674.3 ± 1.4°C for 3.16 h
14	68, 69, 70, 71, 72, 73	635°C for 6 h	634.6 ± 1.5°C for 6 h

[a] PWHT 12 was repeated.

sults of various metallurgical reactions. The relative magnitude of these changes is, of course, dependent on the steel composition and microstructure. Steels containing V or Nb derive some of their strength from finely distributed carbides or carbonitrides of these elements. Vanadium and niobium carbonitrides are dissolved in austenite at high peak temperatures during the weld thermal cycle. Particles that do not reprecipitate upon cooling can precipitate during subsequent subcritical thermal cycles or during PWHT. Therefore, the hardness of the HAZ in V/Nb bearing steels sometimes increases following PWHT due to V/Nb carbonitride precipitation. Because the solution temperature of vanadium carbonitrides is lower than that of niobium carbonitrides, and because niobium is more likely than vanadium to precipitate in the austenite during cooling, it would be expected that vanadium steels would be more susceptible than niobium steel to PWHT hardening (Ref. 2, 4, 5). Therefore, it is important to determine the effect of PWHT on the HAZ of microalloyed steels in a case by case approach.

Gleeble weld thermal simulation is an inexpensive, simple, and rapid test method to investigate fundamental phenomena that take place in the HAZ of a welded joint using a large number of specimens. It is used to simulate the weld thermal cycle under laboratory conditions in order to obtain information about microstructural and property changes in the HAZ. Although, in principle, these changes can be observed and measured from real welds, in practice it is more convenient to work with test pieces representative of one, not a range, of microstructures and grain sizes.

In this experimental work, the effect of weld cooling rates representing a broad range of welding conditions and PWHT schedules, different holding temperatures and holding times, on the microstructure and hardness of Gleeble-simulated CGHAZ of a V-microalloyed X60 steel pipe were evaluated. Additionally, tensile properties and resistance to SSC of CGHAZ with selected hardness levels were determined as well.

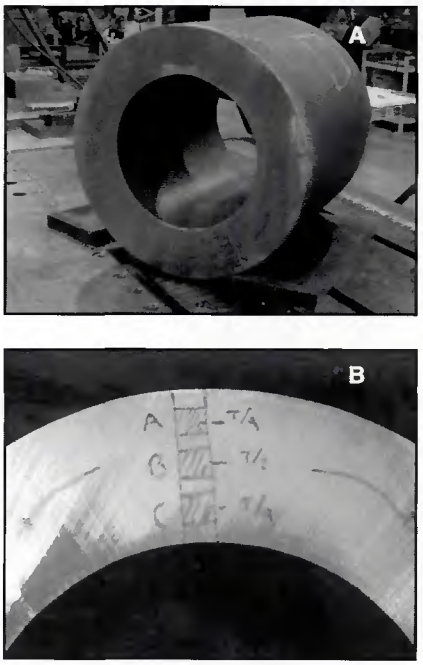

Fig. 2 — A — General view of V-Nb microalloyed X60 steel pipe section; B — through-thickness location of samples for Gleeble simulation and testing.

Experimental Procedures

Materials

The material specimens were machined from a 12.75-in. OD × 64-mm (2.5-in.) wall thickness V-microalloyed seamless X60 steel pipe. Figure 2A and B show a general view of the V-microalloyed X60 steel pipe section used for the experimen-

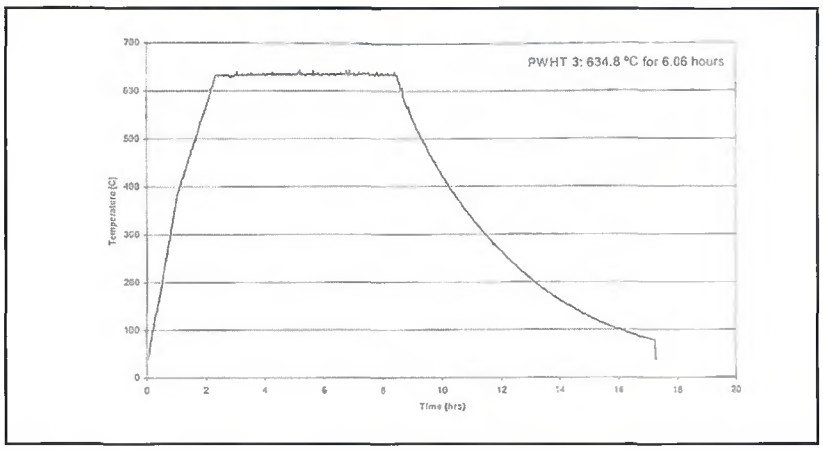

Fig. 3 — Thermal cycle representing one of the PWHT schedules.

tal work, and the relative through-thickness location of the test specimens, respectively. The chemical composition reported in the mill test report (MTR) of the V-microalloyed seamless X60 steel pipe is shown in Table 1.

Gleeble Weld Thermal Cycle Simulation

Single CGHAZ thermal cycles were simulated on 10- × 10- × 55-mm specimens. The thermal cycles were measured using fine k-type thermocouples. The thermocouples were percussion welded to the samples. After the thermocouples were attached, the specimens were clamped between water-cooled jaws of a Gleeble machine, which, in addition to serving as grips to hold the samples, provide a means for introducing the current to the specimen during heating and ensuring a rapid cooling when the current flow is interrupted. Coarse-grained heat-affected zones thermal cycles with a peak temperature of 1320°C (2408°F) and cooling rates ranging from 5 to 80°C/s through the temperature range of 800° to 500°C were imposed on the V-microalloyed X60 steel pipe specimens using the Gleeble simulator.

Postweld Heat Treatment

Following HAZ simulation, CGHAZ samples with a nominal "as-welded" hardness of 280, 300, 325, and 350 HVN-10 were subjected to the specified PWHT cycles listed in Table 2. During PWHT, the heating and cooling rates above 427°C (800°F) were maintained under and close to 400°F/h and 500°F/h, respectively. The furnace used to run the PWHT allowed a close temperature control (± 5°C or less) during the PWHT cycles. Figure 3 shows a thermal cycle representing one of the PWHT schedules used during this study.

Microstructure and Microhardness Evaluation

After HAZ simulation or PWHT, the samples were cross sectioned, mounted, polished, and etched for microstructural evaluation and microhardness testing. Five microhardness readings were obtained from the cross section of each sample.

Tensile Testing of Simulated CGHAZ

Tensile tests were conducted in selected CGHAZ samples in the simulated "as-welded" and in the PWHT condition. The CGHAZ tensile samples that were tensile tested have an average hardness of 300 HV-10 in the simulated "as-welded" condition and an average hardness of 250 HV-10 after being PWHT at 635°C for 6 hours. For the tensile specimens, single CGHAZ thermal cycles were simulated on 10- × 10- × 110-mm specimens. Tensile subsize specimens with a gauge of 0.25 in. (6.35 mm) in diameter × 1 in. (25.4 mm) in length were used.

SSC Testing of a Simulated CGHAZ

Specimens representing a CGHAZ in the PWHT condition were tested in a sour environment according to the procedure specified in NACE TM0177 (Method A) (Ref. 6). The simulated "as-welded" CGHAZ samples exhibited an average hardness of 300 HV-10. The average and maximum hardness of the samples after being subjected to a PWHT at 635°C for 6 hours was 250 and 264 HV-10, respectively. The specimens for SSC were prepared by imposing CGHAZ thermal cycles on 11- × 11- × 110-mm samples. After PWHT, round cross-section test specimens were manufactured from the square bars. The specimens had a gage diameter of 0.250 in. and a gauge length of 1.0 in.,

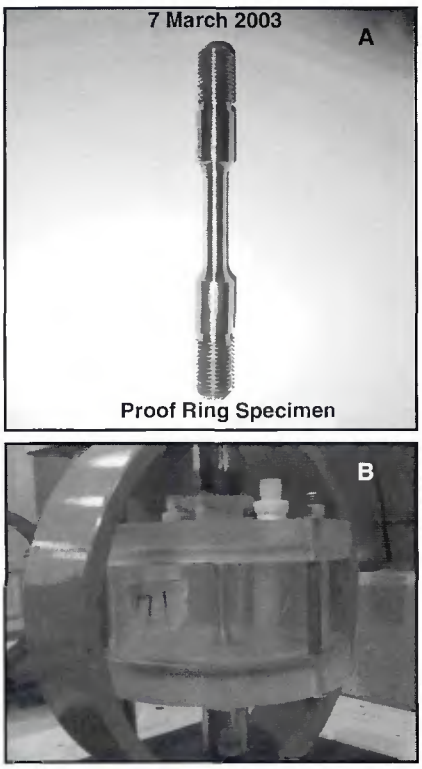

Fig. 4 — A — Round-bar specimen for proof-ring testing in sour environment; B — general view of the proof-ring setup.

as shown in Fig. 4A.

The specimens were stressed to 90% (54 ksi) of the specified minimum yield strength (60 ksi) of the steel pipe using a proof ring setup. Figure 4B shows a general view of the setup of the proof ring. The proof rings were calibrated. The stress level was determined by measuring the deflection of the proof rings. Immediately after applying the stress, the specimens were exposed to a test solution of 5.0 wt% NaCl and 0.5 wt% glacial acetic acid in deionized water for 30 days. The solution was deaerated and purged with H_2S gas in accordance with NACE TM0177 (Method A). The pH of the solution at the beginning was adjusted to 2.7. No pH adjustment was made during the test. The pH of the solution at the end of the test was measured as between 3 and 4, which is within the specification of TM0177 (Method A).

After 30 days, both specimens were removed from the test cells. The external surface of the samples was evaluated for presence of cracks using a binocular microscope at magnification of up to 30X.

Experimental Results and Discussions

Effect of Cooling Rate on CGHAZ Hardness and Microstructure

The resulting CGHAZ microhardness was measured first by making indentations

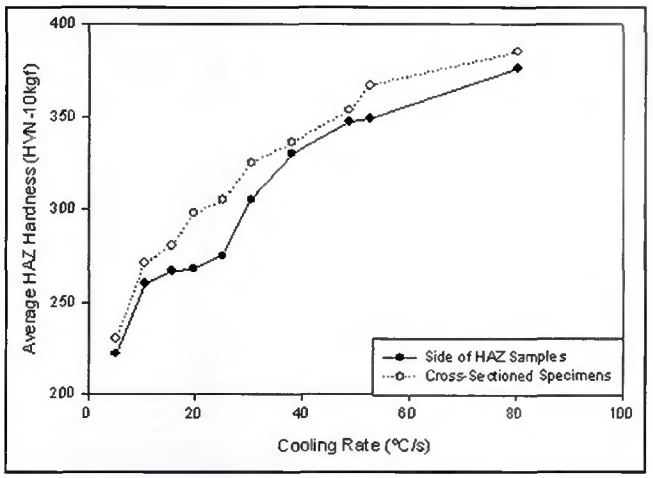

Fig. 5 — Average HAZ hardness as function of cooling rate (data obtained from different specimen preparations).

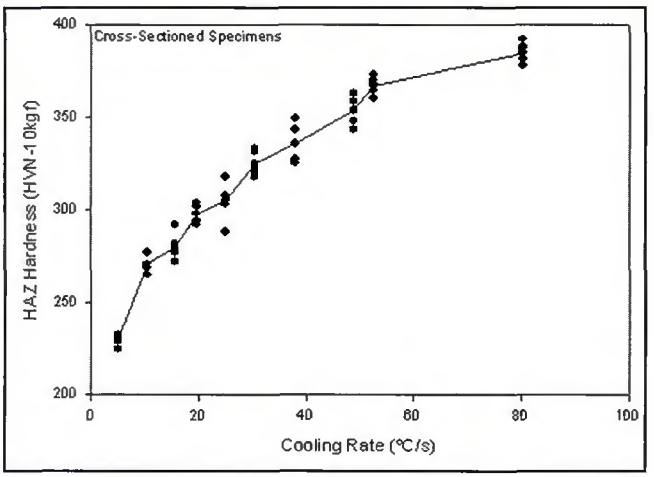

Fig. 6 — HAZ hardness as a function of cooling rate (data obtained from the cross-section of the HAZ specimens after complete metallographic preparation)

Table 3 — Average and Maximum CGHAZ Hardness as Function of Cooling Rate

Specimen	Cooling from 800° to 500°C °C/s	Δt_{8-5} (s)	Average Hardness (HVN-10 kgf)	Maximum Hardness (HVN-10 kgf)	Yurioka Method Prediction
10	5.1	58.94	230	233	229
1	10.5	28.56	271	277	246
37	15.6	19.23	286	294	262
11	15.7	19.13	280	292	262
6	19.7	15.20	298	304	275
46	19.7	15.24	310	316	275
7	25.1	11.94	305	318	290
56	30.3	9.9	331	339	303
2	30.5	9.84	325	333	303
8	38.1	7.88	336	350	320
3	48.8	6.14	353	363	338
9	52.6	5.70	367	373	343
4	80.2	3.74	385	392	368

on the four sides of the Gleeble specimens. After that, each sample was cross sectioned, mounted, polished, and etched. Five microhardness readings were obtained from the cross section of each sample.

It was observed that the hardness data obtained from the cross section of the specimens present a lower level of scattering than the data obtained from the side of the samples. This is the result of a better and smoother surface condition of the samples that were cross sectioned, mounted, polished, and etched. Additionally, the average hardness obtained from the cross sections is higher than the average hardness obtained from the side of the specimens as shown in Fig. 5. This can be explained based on the roughness of the samples. For a given hardness, as the roughness of the samples increases, the size of the indentation will increase. This

Table 4 — Average HAZ Hardness and HAZ Hardness Range Obtained with Selected Cooling Rates

HAZ Cooling from 800° to 500°C HVN-10 kgf		Sample	Hardness Range,	Average HAZ Hardness, HVN-10 kgf	Target HAZ Hardness, HVN-10 kgf
°C/s	Δt_{8-5} (s)				
15.7	19.1	11	272–292	280	280
		37	277–294	286	280
19.7	15.2	6	292–304	298	300
		46	304–315	310	300
30.5	9.8	2	318–333	325	325
		56	312–339	332	325
48.8	6.1	3	343–363	353	350
		66	343–360	354	350
None	None	Base Metal	206–206.5	206	—

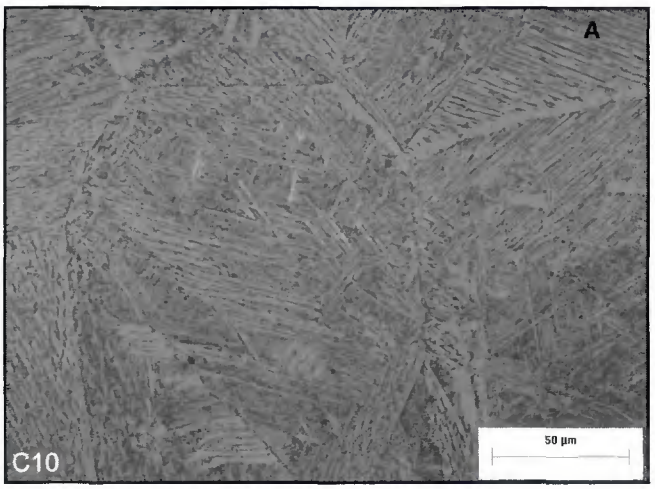

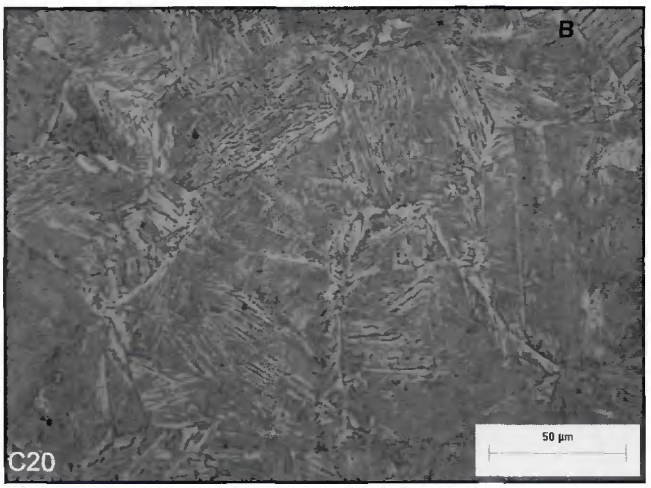

Fig. 7 — "As-welded" microstructure of the CGHAZ in the V-Nb microalloyed X60 steel pipe that resulted at different cooling rates. A — 10°C/s; B — 20°C/s; C — 50°C/s; D — 80°C/s.

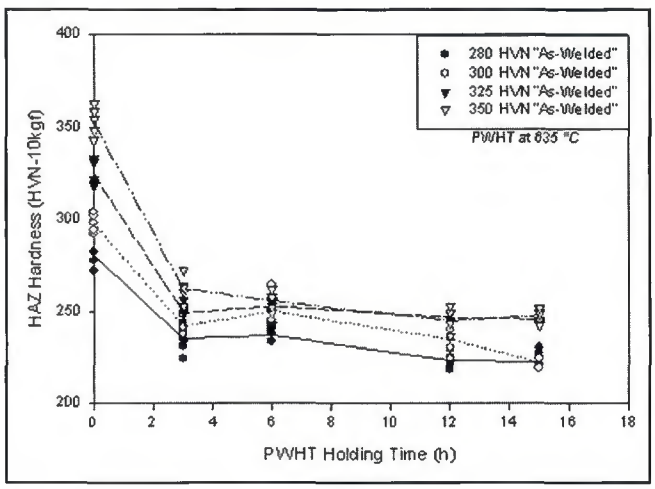

Fig. 8 — Microhardness of simulated HAZ as function of original CGHAZ hardness and PWHT holding time at 635°C.

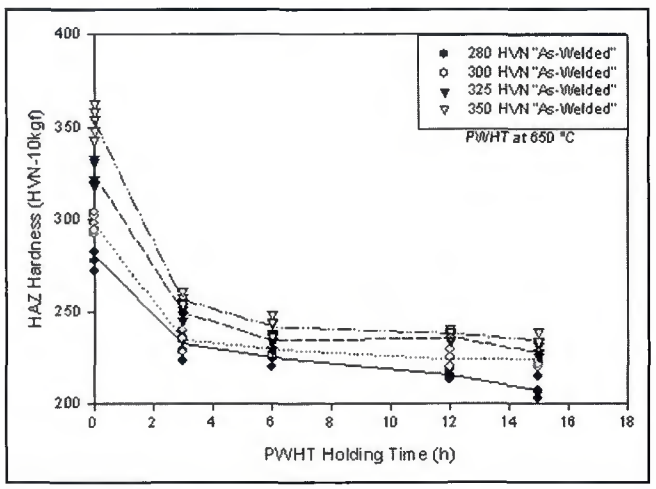

Fig. 9 — Microhardness of simulated HAZ as function of original CGHAZ hardness and PWHT holding time at 650°C.

will result in a lower apparent hardness of the material. The average and maximum CGHAZ hardnesses as functions of the cooling rate from the data obtained from the cross section of the samples are listed in Table 3.

One of the most popular empirical equations that has been developed to predict maximum HAZ hardness as function of composition and cooling rates through the transformation temperature range is the Yurioka method (Ref. 7). The maximum HAZ hardness predicted by the Yurioka method is included in Table 3. It was noted that the measured maximum CGHAZ hardness is generally greater than the predicted maximum hardness. Therefore, the predictions of the Yurioka method are unconservative for the specific V-microalloyed steel used in this study.

A correlation between CGHAZ cooling rate and CGHAZ microhardness, HVN-10, obtained from the cross section of the samples was determined as shown in Fig. 6. It was observed that the maximum hardness of the CGHAZ increases from 233 to 392 HVN-10 as the cooling rates through the temperature range of 800° to 500°C increases from 5° to 80°C/s. The change of hardness as function of cooling rate is the result of the expected change of the CGHAZ microstructure as a function of the cooling rate. The microstructure of CGHAZ was observed to change from mainly a mixture of grain boundary ferrite and ferrite with aligned second phases with a small fraction of upper and lower bainite resulting from cooling rates in the range of 5° to 30°C/s to a microstructure with an increasing fraction of martensite and decreasing fraction of Ferrite, resulting from cooling rates in the range of 40° to 80°C/s. Figure 7A–D shows representative microstructures observed in the CGHAZ of the V-microalloyed seamless X60 steel pipe at different cooling rates through the temperature range of 800° to 500°C.

Response of Gleeble-Simulated CGHAZ to PWHT

In order to evaluate the response of Gleeble simulated CGHAZ to PWHT, HAZ cooling rates of 15.7, 19.7, 30.5, and 48.8°C/s were used to induce nominal CGHAZ hardness of 280, 300, 325, and 350 HVN-10, respectively. The average and HAZ hardness ranges obtained in the CGHAZ with these cooling rates are listed in Table 4. The hardness of the base metal is included in Table 4 as a reference.

CGHAZ Hardness

The microhardness of the CGHAZ as a function of original hardness, PWHT temperature, and holding time are shown in Figs. 8–10. The average and maximum hardness of each one of the tested samples are also listed in listed in Table 5.

None of the PWHT schedules used in

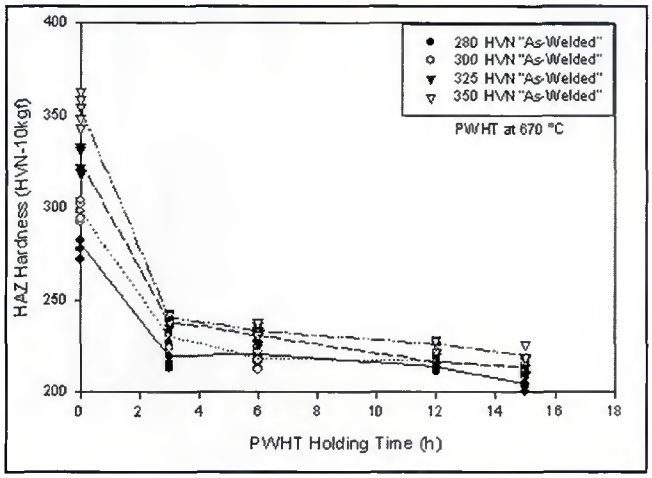

Fig. 10 — Microhardness of simulated HAZ as function of original CGHAZ hardness and PWHT holding time at 670°C.

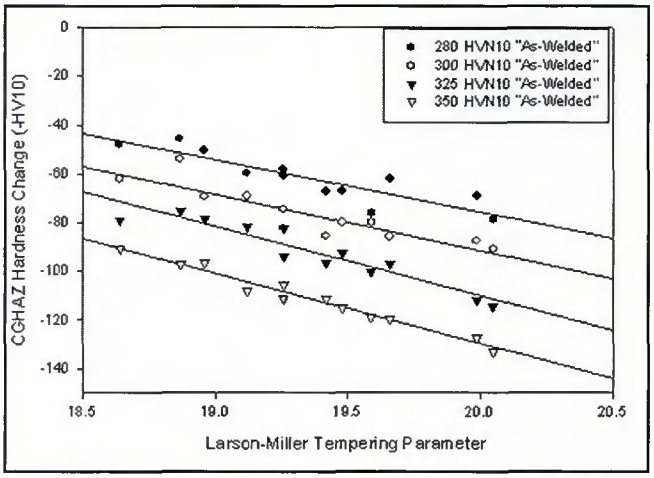

Fig. 11 — Change of the CGHAZ hardness, tempering effect, as function of the as-welded hardness and the Larson-Miller tempering parameter

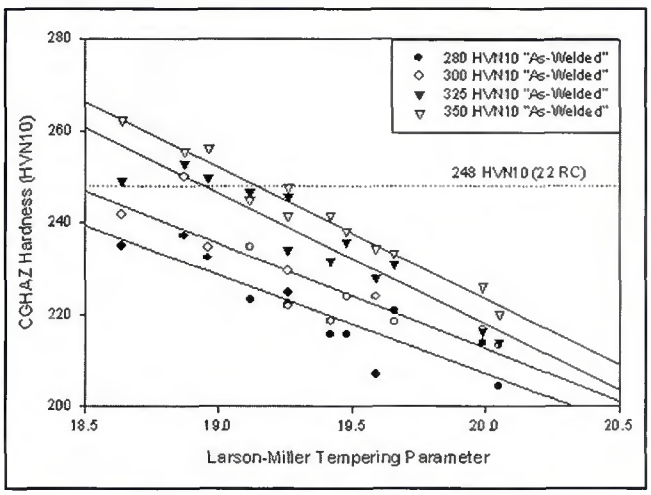

Fig. 12 — Hardness of the CGHAZ as function of the as-welded hardness and the Larson-Miller tempering parameter.

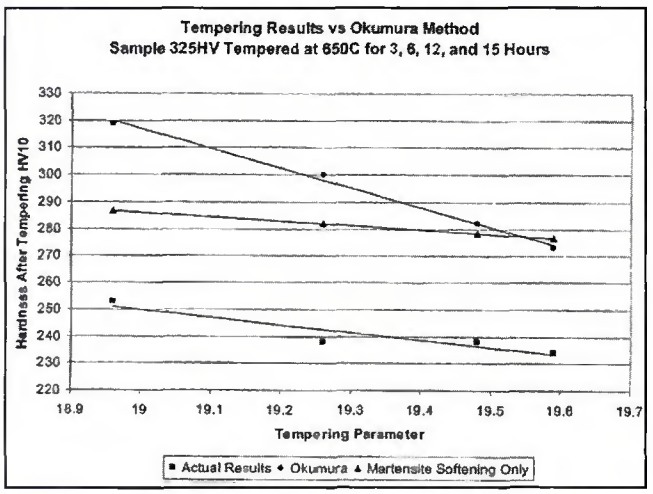

Fig. 13 — Comparison of predicted CGHAZ hardness with actual CGHAZ hardness of the V-microalloyed X60 steel pipe after PWHT.

this study induced any apparent hardening on the CGHAZ of the V-microalloyed X60 steel pipe tested. Age hardening may occur during PWHT and a net increase in hardness will be seen only if precipitation hardening is great enough to offset the microstructural softening that occurs simultaneously during aging. In a PWHT process, recovery of ferrite, decrease in dislocation density, coarsening and spheroidization of cementite, and the microstructural changes in other constituents such as martensite and bainite may also take place, contributing to softening of the material. The net hardness changes in the CGHAZ during PWHT result from the contribution of all the softening and hardening mechanisms and their interplay. The relative magnitude of such changes is, of course, dependent on the steel composition and microstructure, and any effects of PWHT on hardness, and other properties, will be specific to the steel type tested.

As shown in Figs. 8–10, the change of hardness as a function of time at a given holding temperature indicates a higher softening rate, slope, for holding times shorter than 3 hours than the softening rate observed for holding times between 3 to 15 hours. This may result from different hardening and softening mechanisms interacting and being operative at short and long holding times, as discussed in the following sections.

Figure 11 shows the change of hardness in the CGHAZ in the V-microalloyed X60 steel pipe as a function of the Larson-Miller tempering parameter. The tempering effect or change of hardness in the CGHAZ during PWHT depends not only in temperature and time, but also on the original hardness of the CGHAZ. The tempering effect of a given PWHT increases with an increase in the as-welded hardness of the CGHAZ. However, in Figs. 8–10, it is observed that most of the decrease in hardness happens relatively early in the PWHT, holding times equal or less than 3 hours. At low tempering parameter values, the tempering effect of a given PWHT increases with an increase in the as-welded hardness of the CGHAZ. This behavior may be related to tempering of an increasing martensite/bainite volume fraction present in the CGHAZ as the "as-welded" hardness increases. Additionally, a harder "as-welded" CGHAZ resulting from faster cooling rate is expected to have a higher dislocation density and a higher thermodynamic driving force for tempering.

On the other hand, the PWHTs with holding times between 3 and 15 hours resulted in roughly similar slopes of hardness change per unit of tempering parameter change, e.g., nearly parallel lines, independent of the original CGHAZ hardness, as seen in Fig. 11. It is generally

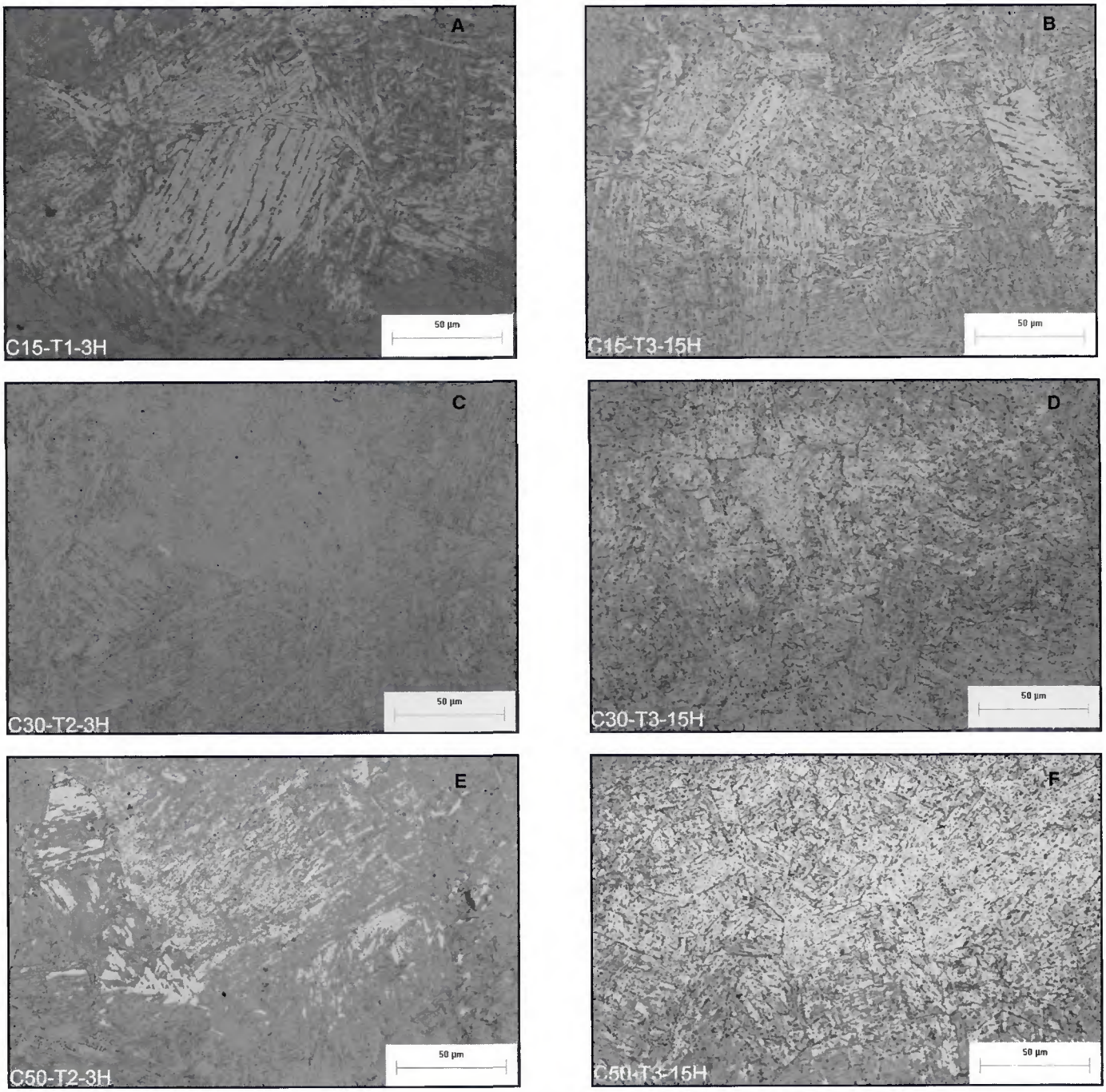

Fig. 14 — Representative microstructures of the CGHAZ after PWHT. A — 15°C/s , PWHT at 635°C for 3 hours; B — 15°C/s , PWHT at 670°C for 15 hours; C — 30°C/s , PWHT at 650°C for 3 hours; D — 30°C/s , PWHT at 670°C for 15 hours; E — 50°C/s , PWHT at 650°C for 3 hours; F — 50°C/s , PWHT at 670°C for 15 hours.

expected that faster cooling rates would result in higher vanadium supersaturation of the CGHAZ. Therefore, CGHAZ induced with faster cooling rates should exhibit stronger secondary hardening. However, no obvious secondary hardening was observed in any of the CGHAZ evaluated. Had hardness changes during tempering been dominated by secondary hardening from vanadium carbide precipitates, a nonlinear curve would be expected.

As shown in Figs. 11 and 12, for PWHT times between 3 and 15 hours, the interaction of time and temperature in reducing the hardness of the CGHAZ during PWHT can be described by the Larson-Miller tempering parameter, P, given by the following equation:

$$P = T\,(C + \log t) \times 10^{-3} \qquad (1)$$

where T is the absolute temperature of PWHT in degree Kelvin, t is the PWHT time in hours, and C is a constant equal approximately to 20. The Larson-Miller tempering parameter of each PWHT is listed in Table 6. The Larson-Miller tempering parameter was originally devised as an indicator of the tempering behavior via a single reaction (Refs. 8, 9). Therefore, in the present case, there is clearly an indication that the tempering behavior of the CGHAZ in the V-microalloyed seamless X60 steel pipe at the holding temperatures used in this study and for holding times between 3 and 15 hours is controlled by a single metallurgical reaction. This may indi-

Table 5 — Change of CGHAZ Hardness (HVN-10 kgf) as Function of PWHT Temperature and Holding Time

Holding Time (h)	Holding Temperature 635°C		650°C		670°C	
	Nominal Hardness in the "As-Welded" Condition: 280					
	Average Hardness	Maximum Hardness	Average Hardness	Maximum Hardness	Average Hardness	Maximum Hardness
0	280.2	292.0	280.2	292.0	280.2	292.0
3	235.0	244.0	232.4	239.0	215.6	222.0
6	237.2	241.0	224.6	227.0	220.7	227.5
12	223.2	229.0	215.6	218.0	213.8	218.0
15	222.3	230.0	206.8	215.0	204.4	210.0
	Nominal Hardness in the "As-Welded" Condition: 300					
	Average Hardness	Maximum Hardness	Average Hardness	Maximum Hardness	Average Hardness	Maximum Hardness
0	298.0	304	298.0	304.0	298.0	304.0
3	241.8	248.0	234.6	240.0	218.6	228.0
6	250.0	264.0	229.5	237.0	218.4	225.0
12	234.8	245.0	223.8	229.0	216.7	222.0
15	221.8	225.0	223.8	233.0	213.2	218.0
	Nominal Hardness in the "As-Welded" Condition: 325					
	Average Hardness	Maximum Hardness	Average Hardness	Maximum Hardness	Average Hardness	Maximum Hardness
0	325.0	333.0	325.0	333.0	325.0	333.0
3	249.0	256.0	249.6	253.0	231.6	235.0
6	252.8	258.0	233.9	238.0	230.9	236.0
12	246.6	253.0	235.6	238.0	216.3	219.0
15	245.6	249.0	227.8	234.0	213.7	218.5
	Nominal Hardness in the "As-Welded" Condition: 350					
	Average Hardness	Maximum Hardness	Average Hardness	Maximum Hardness	Average Hardness	Maximum Hardness
0	353.4	363.0	353.4	363.0	353.4	363.0
3	262.4	272.0	256.4	261.0	241.6	243.0
6	255.6	262.0	241.6	248.0	233.4	238.0
12	244.8	253.0	238.0	241.0	226.0	229.0
15	247.7	252.0	234.2	239.0	220.1	226.0

cate that at long holding times, the softening mechanism becomes independent of starting hardness and microstructure. In this condition, tempering of the CGHAZ may be approaching a purely carbide coarsening dominated mechanism as observed in the last stages of tempering of a martensitic microstructure.

Different methods have been developed to predict the effect of PWHT on HAZ hardness. One of these methods is the Okumura method, which has been developed to combine martensite softening with hardening caused by V, Nb, and Mo all as a function of tempering parameter, martensite fraction, and composition (Refs. 5, 10).

A comparison between the prediction of the Okumura methods and observed CGHAZ hardness is shown in Fig. 13. In this case, the effect of PWHT at 650°C for 3, 6, 12, and 15 hours on the CGHAZ hardness of samples with simulated "as-welded" hardness of 325HV is compared to the hardness values predicted by the Okumura method. Results show actual CGHAZ hardness being significantly below the predicted value; however, the difference narrows as tempering parameter increases. These results indicate that for the specific X60 material tested in this study, the Okumura equation significantly over predicts hardness at a given tempering parameter. The slope of the predicted value curve which includes the combined effect of martensite softening and precipitation hardening is much steeper than the actual data. Additionally, the actual CGHAZ hardness data follows a similar trend that the prediction for tempering controlled by martensite softening only. This also confirms the absence of secondary hardening as major reaction during the tempering process of the CGHAZ of the V-microalloyed steel pipe. However, the actual data presents a slope that is steeper than pure martensite softening, but not as steep as that predicted by the Okumura equation,which may indicate retardation of softening of the CGHAZ due to minor precipitation reaction.

Figure 12 shows the hardness of the CGHAZ in the V-microalloyed X60 steel pipe as function of the Larson-Miller tempering parameter. As indicated in Fig. 12, PWHT with a characteristic Larson-Miller tempering parameter of about 18.47, 18.96, and 19.16 is needed to decrease the hardness of the CGHAZ in the V-microalloyed X60 steel pipe from an as-welded hardness of 300, 325, and 350 HVN-10, respectively, to a hardness of about 248 HVN10. The maximum hardness of 248 HVN-10 (22 RC) recommended by NACE to avoid risk to SSC is included in Fig. 12 as a reference. These results have significant implications for the required control over welding procedure variables. These tempering conditions require much longer holding times during PWHT than the holding time normally required in different industry codes, which are a function of thickness only.

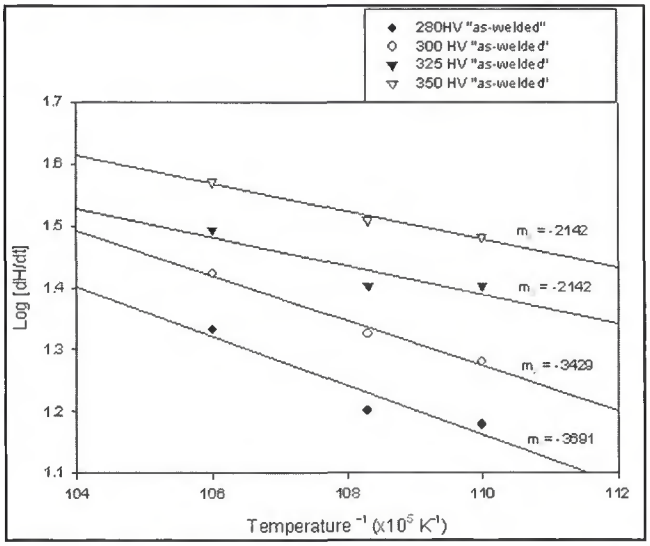

Fig. 15 — Tempering of the CGHAZ during PWHT for 3 hours, log of softening rate (dH/dt) as function of the inverse temperature (1/T).

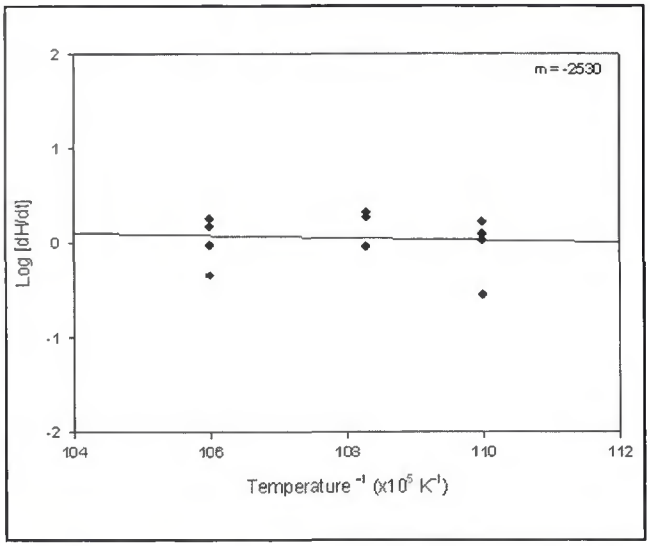

Fig. 16 — Tempering of the CGHAZ during PWHT for 3 to 15 hours, log of softening rate (dH/dt) as function of the inverse temperature (1/T).

CGHAZ Microstructure

Figure 14A–F shows microstructures representative of the CGHAZ induced at different cooling rates and after being subjected to different PWHT. Metallographic examinations showed a small dependence of microstructure on PWHT time, although a stronger effect of temperature was observed, in which the degree of dispersion of the carbides was temperature dependent.

<Insert Fig. 14A–F, Figure 14-a.tif, Figure 14-b.tif, Figure 14-c.tif, Figure 14-d.tif, Figure 14-e.tif, and Figure 14-f.tif>

As previously described, the microstructure of the CGHAZ can be regarded as composed mainly of ferrite with aligned second phases and an increasing fraction of bainite/martensite constituents as the cooling rate is increased. Based on optical microscopic observation, the strongest effect of varying heat treatment temperature was on the morphology of the ferrite with aligned second phases. With increasing temperature, the packets of second phases spheroidize, eventually forming a small number of globular precipitates to minimize the interfacial energy. The elongated constituent would be expected to have a high interfacial energy because of the higher surface area to volume ratio. It seems that during heat treatment, carbon diffusion enables the second phase to dissolve and form smaller packets, as observed by other workers on both base metal (Ref. 11) and weld metal (Ref. 12). At the same time, the low angle boundaries between the ferrite laths became less pronounced.

As PWHT temperature was increased, the intragranular microstructure became less defined. The grain and colony boundaries were more pronounced after PWHT, compared to the "as-welded" condition. From the optical examination, this seemed to be accompanied by carbide formation at colony and possibly prior austenite grain boundaries. This effect has been noted in weld metals (Ref. 13) and, indeed, high angle boundaries are known to be preferred sites for carbide formation both because of a higher carbon diffusion rate along such boundaries and because the high vacancy level more readily accommodates the volume difference between cementite and the ferrite matrix.

Additional fine scale microstructural variations during PWHT, such as martensite decomposition, annealing of dislocations, and V/Nb carbide precipitation that are embodied in the variation in the HAZ hardness data, are beyond the resolution capabilities of optical microscopy.

Metallurgical Reactions Controlling Tempering of CGHAZ

The fact that time and temperature have corresponding effects on tempering of steels as shown in Figs. 8–12 has been known for a long time. The observed time-temperature relation is based on the well known theory of rate processes, which states that the rate at which certain processes progress is related to temperature by activation or Arhennius-type laws. Therefore, their temperature dependence can be described in the form

$$r = Ae^{-Q/RT} \quad (2)$$

where r = rate, A = constant, e = natural logarithm base, Q = apparent activation energy for process, R = gas constant (2 cal/mol/°K), and T = absolute temperature, °K.

Therefore, the apparent activation energy of tempering observed in the CGHAZ was also determined in the present work. The logarithmic form of equation 2 is log (dH/dt) = log A – m 1/T (3) where (dH/dt) is the softening rate and m = Q / 2.3R.

The apparent activation energy for tempering of the CGHAZ during short holding times, less than 3 hours, and during long holding times, 3 to 15 hours, was evaluated by plotting log (dH/dt) as function of 1/T in the form of an Arhennius plot (Figs. 15, 16). The determined values of the apparent activation energy are listed in Table 7.

As expected, the apparent activation energy for tempering of the CGHAZ during short holding times depends on the original microstructure and associated hardness of the CGHAZ. The average apparent activation energy for tempering of CGHAZs that consist of mainly ferrite with aligned second phases was determined to be equal to 16,376 cal/mol. On the other hand, for CGHAZs with a mainly martensitic microstructure, the apparent activation energy for tempering was determined to be equal to 9853 cal/mol. Tempering at temperatures between 635° and 670°C and holding times less than 3 hours are expected to induce different thermally activated metallurgical reactions. These reactions include recovery of dislocations in the ferrite lath boundaries, recrystallization of ferrite grains, transformation of low-carbon martensite to ferrite by losing both its carbon and tetragonality, precipitation of cementite, and coarsening of the second phases. Therefore, it is difficult to associate the apparent activation energy with a specific physical phenomenon or reaction.

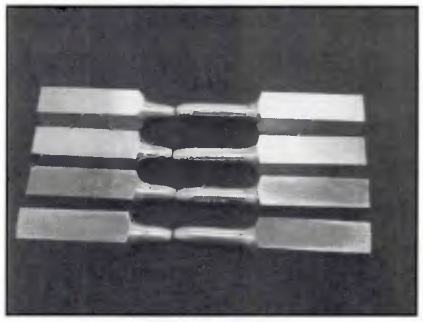

Fig. 17 — Failure location of tensile test samples.

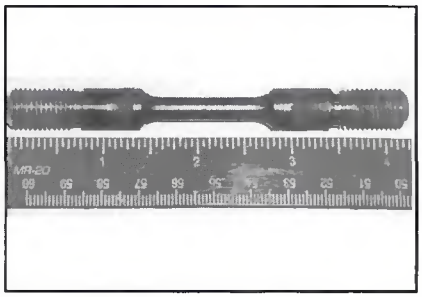

Fig. 18 — CGHAZ specimen after SSC testing.

On the other hand, it was observed that the apparent activation energy for tempering of the CGHAZ during holding times between 3 and 15 hours was independent of the original microstructure and associated hardness of the CGHAZ. The average apparent activation energy for tempering of CGHAZ during long holding times was determined to be equal to 11,636 cal/mol. This makes sense taking into account that after 3 hours of tempering, the microstructure is expected to be an aggregate of ferrite containing a large number of spheroidal carbide and second-phase particles independent of the original microstructure. The coarsening of cementite and second-phase particles is considered to be the primary metallurgical reaction controlling the softening of the CGHAZ during late stages of tempering.

The growth rate of carbide particles in iron-carbon alloys is diffusion-controlled (Ref. 14). The activation energy for the transfer of carbon atoms from cementite to alpha iron is 9700 cal/mol (Ref. 15). The activation energy for the diffusion of carbon atoms in alpha iron is 20,100 cal/mol (Refs. 16, 17). Therefore, it seems that the transfer of carbon atoms from cementite to ferrite is the main controlling mechanism of tempering of the CGHAZ during the late stages of tempering. However, further experimental work is needed to support this statement.

Tensile Properties and SSC Resistance of CGHAZ

Tensile Properties

The results of the tensile tests are reported in Table 8. All the samples seem to have failed in the base metal very close to the interface with the simulated HAZ as shown in Fig. 17. Therefore, the results are not representative of the intrinsic mechanical properties of the simulated CGHAZ. The fracture of all samples has a "cup-cone" feature characteristic of ductile failure. The lower tensile properties of the samples in the as-simulated condition may be due to the normal variance of properties of the base metal from sample to sample and due to the clearly overmatching condition of the HAZ as compared to the base metal. A highly overmatched condition would induce localized deformation in the base metal, which causes the point of instability to be controlled by the properties of the base metal. On the other hand, a lower overmatched condition of the PWHT samples will cause a more homogeneous distribution of the plastic deformation and the point of stability being controlled by the strain hardening behavior of both the HAZ and the base metal. Sample 75 failed at or near a gauge mark, which may have resulted in a stress concentrator and the observed low percent elongation.

SSC Resistance

The PWHT CGHAZ specimens with an average and maximum hardness of 250 and 264 HV-10, respectively, did not rupture in the H_2S environment after 30 days

Table 6 — Larson-Miller Tempering Parameter, P, of different CGHAZ PWHT

PWHT	PWHT Description	P
1	636.4 ± 4.3°C for 15.27 h	19.26
2	634 ± 3.3°C for 12.03 h	19.12
3	634.8 ± 2.5°C for 6.06 h	18.87
4	636.3 ± 4.2°C for 3.16 h	18.64
5	652 ± 1.9°C for 15.25 h	19.59
6	651.1 ± 2.8°C for 12.1 h	19.48
7	653.7 ± 2.2°C for 6.14 h	19.26
8	652.2 ± 2.8°C for 3.14 h	18.96
9	673.7 ± 4.4°C for 15.25 h	20.05
10	675 ± 4.5°C for 12.14 h	19.99
11	672.6 ± 1.7°C for 6.14 h	19.66
12[a]	680 ± 5°C for 3.26 h	—
13[a]	674.3 ± 1.4°C for 3.16 h	19.42
14	634.6 ± 1.5°C for 6 h	18.86

[a] PWHT 12 was repeated.

Table 7 — Apparent Activation Energy for Tempering of the CGHAZ

Regime (Holding time)	Original Characteristics of the CGHAZ (Hardness-Microstructure)	Activation Energy, cal/mol
1 (Less than 3 hours)	280 HVN-Ferrite with aligned second phases	16,979
	300 HVN-Ferrite with aligned second phases	15,773
	325 HVN-Mainly martensite with small fraction of ferrite with aligned second phases	9,853
	350 HVN-Martensite	9,853
2 (3 to 15 hours)	All	11,636

Table 8 — Tensile Test Results of Simulated "As-Welded" and PWHT CGHAZ in V-Microalloyed X60 Steel Pipe

Specimen	Nominal Hardness, HV-10	UTS MP	ksi	0.2 Yield Strength MPa	ksi	Elongation (%)	Reduction of Area (%)
74	300	603.4	87.5	466.2	67.6	30	76.3
75	300	615.9	89.3	482.8	70.0	14.9[a]	76.4
68 (PWHT)	250	628.3	91.1	520.7	75.5	26.1	76.2
69 (PWHT)	250	626.9	90.9	534.5	77.5	26.4	76.6

[a] Sample failed at or very near a gauge mark.

of testing. The specimens had a smooth, black, shiny appearance —Fig. 18. No cracks were visible on the external surface of the gauge length at magnifications up to 30X.

Conclusions

1. The maximum hardness in the CGHAZ of the V-microalloyed X60 steel pipe increases from 233 to 392 HV-10 by increasing the CGHAZ cooling rate through the 800° to 500°C temperature range from 5° to 80°C/s.

2. The microstructure of CGHAZ changes from a mixture of grain boundary ferrite and ferrite with aligned second phases resulting at cooling rates from 5° to 30°C/s to a microstructure with an increasing fraction of martensite at cooling rates from 40° to 80°C/s.

3. CGHAZ cooling rates of 15.7, 19.7, 30.5, and 48.8°C/s induced an average CGHAZ hardness of 280, 300, 325, and 350 HVN-10, respectively.

4. None of the PWHT schedules used in this study induced any apparent hardening on the CGHAZ of the V-microalloyed X60 steel pipe tested.

5. The softening rate of the CGHAZ or tempering effect of PWHT decreases after 3 hours at a given PWHT temperature used in this study.

6. The tempering effect of PWHT on the CGHAZ for holding times between 3 and 15 hours is described by the Larson-Miller tempering parameter. Therefore, the tempering behavior of the CGHAZ is controlled mainly by a single metallurgical reaction.

7. Coarse-grained heat-affected zones in the V-microalloyed X60 steel pipe with an as-welded hardness of 300, 325, and 350 HV-10 need to be subjected to a PWHT with a characteristic Larson-Miller tempering parameter of about 18.47, 18.96, and 19.16, respectively, to decrease the hardness to 248 HVN10. This can have significant impacts on welding procedure qualification requirements.

8. The Yurioka and Okumura methods were not adequate to calculate and predict as-welded hardness and hardness after PWHT for the CGHAZ of the V-microalloyed steel pipe evaluated.

9. The apparent activation energy for tempering of the CGHAZ during short holding times depends on the original microstructure and associated hardness of the CGHAZ. The apparent activation energy for tempering of CGHAZ that consists of ferrite with aligned second phases was equal to 16,376 cal/mol. The apparent activation energy for tempering for CGHAZ with a martensitic microstructure was equal to 9853 cal/mol.

10. The apparent activation energy for tempering of the CGHAZ during holding times between 3 and 15 hours was independent of the original microstructure and associated hardness of the CGHAZ. The average apparent activation energy for tempering of CGHAZ during long holding times was 11,636 cal/mol.

11. The tensile test results were dependent on the degree of overmatching between the CGHAZ and the base metal.

12. The PWHT V-microalloyed X60 steel CGHAZ with an average and maximum hardness of 250 and 264 HV-10, respectively, were resistant to SSC.

References

1. Spaeder, Jr., C. E., and Doty, W. D. 1995. ASME post-weld heat treating practices: An interpretive report. WRC Bulletin, 407.

2. Stout, R. D. December 1985. Postweld heat treatment of pressure vessel steels. WRC Bulletin, 302 February.

3. NACE Standard MR0175, Metals for Sulfide Stress Cracking and Stress Corrosion Cracking Resistance in Sour Oilfield Environment. Houston, Tex.

4. Shiga, C., Gotoh, A., Kojima, T., Fukada, Y., Ikeuti, K., and Matuda, F. 1996. State of the art review on the effect of PWHT on properties of steel weld metal. Welding in the World 37(4): 163–176.

5. Xu, P., Somers, B. R., and Pense, A. W. 1994. Vanadium and columbium additions in pressure vessel steels. WRC Bulletin, 395.

6. NACE Standard TM0177, Laboratory Testing of Metals for Resistance to Sulfide Stress Cracking in H2S Environment. Houston, Tex.

7. Yurioka, N., Okumura, M., Kasuya, T., and Cotton, H. J. U. 1987. Prediction of HAZ hardness of transformable steels. Metal Construction 119: 217R–223R.

8. Larson, F. R., and Miller, J. 1952. A time-temperature relationship for rupture and creep stresses. ASME 74: 765–775.

9. Holloman, J. H., and Jaffee, L. D. 1945. Time and temperature relations in tempering steel. Trans. AIME 162: 223–249.

10. Okumura, M., Yurioka, N., Kasuya, T., and Cotton, H. J. 1987. Prediction of HAZ hardness after PWHT. Proceedings of International Conference on Stress Relieving Heat Treatments of Welded Steel Constructions, (7): 61–68. Sofia, Bulgaria.

11. Cochrane, R. C. 1971. Some effects of carbide particles size on the Charpy impact behavior of normalized and stress relieved C-Mn steels. The Iron and Steel Institute, 3: 101–106.

12. Billy, J., Johansson, T., Loberg, B., and Easterling, K. E. 1980. Stress Relief heat treatment of submerged-arc welded microalloyed steels. Metal Technology 7(2): 67–78.

13. Farrar, R. A., Taylor, L. G., and Harrison, E. M. 1979. Effect of stress relieving on fracture properties of submerged-arc welds of C-Mn Steels. Metals Technology 6(10): 380–389.

14. Vedula, K. M., and Heckel, R. W. 1970. Spheroidization of binary Fe-C alloys over a range of temperatures. Met. Trans 1(1): 9.

15. Wert, C. A. 1950. Solid Solubility of Cementite in alpha iron. trans. AIME 188(10): 1242–1244.

16. Wert, C. A. 1950. Diffusion coefficient of C in α-Iron. Phys. Rev. 79(4): 601.

17. Wert, C. A., and Zener, C. 1949. Interstitial atomic diffusion coefficients. Phys. Rev. 76(8): 1169.